Published in "Optics Express 17(16): 13904-13917, 2009"
which should be cited to refer to this work.

Dynamic laser speckle imaging of cerebral blood flow

P. Zakharov [1,2], A.C. Völker [1], M.T. Wyss [3,4], F. Haiss [4], N. Calcinaghi [4], C. Zunzunegui [4], A. Buck [3], F. Scheffold [1] and B. Weber [4 *]

[1] *Department of Physics, University of Fribourg, 1700 Fribourg, Switzerland*
[2] *Solianis Monitoring AG, 8050 Zürich, Switzerland*
[3] *Division of Nuclear Medicine, University Hospital Zurich, 8091 Zurich, Switzerland*
[4] *Institute of Pharmacology and Toxicology, University of Zurich, 8091 Zurich, Switzerland*
** bweber@pharma.uzh.ch*

Abstract: Laser speckle imaging (LSI) based on the speckle contrast analysis is a simple and robust technique for imaging of heterogeneous dynamics. LSI finds frequent application for dynamical mapping of cerebral blood flow, as it features high spatial and temporal resolution. However, the quantitative interpretation of the acquired data is not straightforward for the common case of a speckle field formed by both by moving and localized scatterers such as blood cells and bone or tissue. Here we present a novel processing scheme, we call dynamic laser speckle imaging (dLSI), that can be used to correctly extract the temporal correlation parameters from the speckle contrast measured in the presence of a static or slow-evolving background. The static light contribution is derived from the measurements by cross-correlating sequential speckle images. In-vivo speckle imaging experiments performed in the rodent brain demonstrate that dLSI leads to improved results. The cerebral hemodynamic response observed through the thinned and intact skull are more pronounced in the dLSI images as compared to the standard speckle contrast analysis. The proposed method also yields benefits with respect to the quality of the speckle images by suppressing contributions of non-uniformly distributed specular reflections.

References and links

1. C. Ayata, H. K. Shin, S. Salomone, Y. Ozdemir-Gursoy, D. A. Boas, A. K. Dunn, and M. A. Moskowitz, "Pronounced hypoperfusion during spreading depression in mouse cortex," J. Cereb. Blood Flow Metab. **24**(10), 1172–1182 (2004).
2. J. D. Briers, "Laser Doppler, speckle and related techniques for blood perfusion mapping and imaging," Physiol. Meas. **22**(4), R35–R66 (2001).
3. A. K. Dunn, H. Bolay, M. A. Moskowitz, and D. A. Boas, "Dynamic imaging of cerebral blood flow using laser speckle," J. Cereb. Blood Flow Metab. **21**(3), 195–201 (2001).
4. A. K. Dunn, A. Devor, H. Bolay, M. L. Andermann, M. A. Moskowitz, A. M. Dale, and D. A. Boas, "Simultaneous imaging of total cerebral hemoglobin concentration, oxygenation, and blood flow during functional activation," Opt. Lett. **28**(1), 28–30 (2003).
5. T. Durduran, M. G. Burnett, G. Q. Yu, C. Zhou, D. Furuya, A. G. Yodh, J. A. Detre, and J. H. Greenberg, "Spatiotemporal quantification of cerebral blood flow during functional activation in rat somatosensory cortex using laser-speckle flowmetry," J. Cereb. Blood Flow Metab. **24**(5), 518–525 (2004).
6. J. S. Paul, H. Al Nashash, A. R. Luft, and T. M. Le, "Statistical mapping of speckle autocorrelation for visualization of hyperaemic responses to cortical stimulation," Ann. Biomed. Eng. **34**(7), 1107–1118 (2006).
7. B. Weber, C. Burger, M. T. Wyss, G. K. von Schulthess, F. Scheffold, and A. Buck, "Optical imaging of the spatiotemporal dynamics of cerebral blood flow and oxidative metabolism in the rat barrel cortex," Eur. J. Neurosci. **20**(10), 2664–2670 (2004).
8. A. B. Parthasarathy, W. J. Tom, A. Gopal, X. J. Zhang, and A. K. Dunn, "Robust flow measurement with multi-exposure speckle imaging," Opt. Express **16**(3), 1975–1989 (2008).

9. P. Zakharov, A. Völker, A. Buck, B. Weber, and F. Scheffold, "Quantitative modeling of laser speckle imaging," Opt. Lett. **31**(23), 3465–3467 (2006).
10. H. Cheng, Q. Luo, S. Zeng, S. Chen, J. Cen, and H. Gong, "Modified laser speckle imaging method with improved spatial resolution," J. Biomed. Opt. **8**(3), 559–564 (2003).
11. H. Y. Cheng, and T. Q. Duong, "Simplified laser-speckle-imaging analysis method and its application to retinal blood flow imaging," Opt. Lett. **32**(15), 2188–2190 (2007).
12. P. C. Li, S. L. Ni, L. Zhang, S. Q. Zeng, and Q. M. Luo, "Imaging cerebral blood flow through the intact rat skull with temporal laser speckle imaging," Opt. Lett. **31**(12), 1824–1826 (2006).
13. D. D. Duncan, and S. J. Kirkpatrick, "Can laser speckle flowmetry be made a quantitative tool?" J. Opt. Soc. Am. A **25**(8), 2088–2094 (2008).
14. T. Smausz, D. Zölei, and B. Hopp, "Real correlation time measurement in laser speckle contrast analysis using wide exposure time range images," Appl. Opt. **48**(8), 1425–1429 (2009).
15. A. C. Völker, P. Zakharov, B. Weber, F. Buck, and F. Scheffold, "Laser speckle imaging with an active noise reduction scheme," Opt. Express **13**(24), 9782–9787 (2005).
16. P. Zakharov, S. Bhat, P. Schurtenberger, and F. Scheffold, "Multiple-scattering suppression in dynamic light scattering based on a digital camera detection scheme," Appl. Opt. **45**(8), 1756–1764 (2006).
17. A. F. Fercher, and J. D. Briers, "Flow Visualization by Means of Single-Exposure Speckle Photography," Opt. Commun. **37**(5), 326–330 (1981).
18. B. J. Berne, and R. Pecora, *Dynamic Light Scattering. With Applications to Chemistry, Biology, and Physics.* (Dover Publications, New York, 2000).
19. P. Zakharov, A. Volker, A. Buck, B. Weber, and F. Scheffold, "Non-ergodicity correction in laser speckle biomedical imaging," Proc. SPIE **6631**, 66310D (2009).
20. J. D. Briers, G. Richards, and X. W. He, "Capillary blood flow monitoring using laser speckle contrast analysis (LASCA)," J. Biomed. Opt. **4**(1), 164–175 (1999).
21. P. Zakharov, and F. Scheffold, *Advances in dynamic light scattering techniques in Light Scattering Reviews 4* (Springer, Heidelberg, 2009).
22. D. A. Boas, and A. G. Yodh, "Spatially varying dynamical properties of turbid media probed with diffusing temporal light correlation," J. Opt. Soc. Am. A **14**(1), 192–215 (1997).
23. S. Yuan, A. Devor, D. A. Boas, and A. K. Dunn, "Determination of optimal exposure time for imaging of blood flow changes with laser speckle contrast imaging," Appl. Opt. **44**(10), 1823–1830 (2005).
24. P. Apollo, Y. Wong, and P. Wiltzius, "Dynamic light scattering with a ccd camera," Rev. Sci. Instrum. **64**(9), 2547–2549 (1993).
25. R. Bandyopadhyay, A. S. Gittings, S. S. Suh, P. K. Dixon, and D. J. Durian, "Speckle-visibility spectroscopy: A tool to study time-varying dynamics," Rev. Sci. Instrum. **76**(9), 093110 (2005).
26. V. Tuchin, *Tissue Optics: Light Scattering Methods and Instruments for Medical Diagnosis, Second Edition* (SPIE Press, Bellingham, 2007).
27. J. Berwick, D. Johnston, M. Jones, J. Martindale, P. Redgrave, N. McLoughlin, I. Schiessl, and J. E. Mayhew, "Neurovascular coupling investigated with two-dimensional optical imaging spectroscopy in rat whisker barrel cortex," Eur. J. Neurosci. **22**(7), 1655–1666 (2005).
28. A. Devor, A. K. Dunn, M. L. Andermann, I. Ulbert, D. A. Boas, and A. M. Dale, "Coupling of total hemoglobin concentration, oxygenation, and neural activity in rat somatosensory cortex," Neuron **39**(2), 353–359 (2003).
29. U. Lindauer, A. Villringer, and U. Dirnagl, "Characterization of CBF response to somatosensory stimulation: model and influence of anesthetics," Am. J. Physiol. **264**(4 Pt 2), H1223–H1228 (1993).

Introduction

Functional imaging of the brain has become a field of intensive research since noninvasive methods, such as functional magnetic resonance imaging (fMRI) and positron emission tomography (PET) have been introduced in neuroscience. However, the spatial resolution of these techniques is limited (ca. 1-5 mm). Thus, the development of novel optical approaches has been pursued, as these offer a resolution down to the micron scale, which is required for a fundamental understanding of brain functioning. Moreover, optical imaging benefits from the rapid development of laser sources and optoelectronic detection devices. In parallel with a rapid technological progress, the cost of these devices is continuously decreasing. Compared to fMRI and PET optical techniques are thus relatively inexpensive tools. The hemodynamic response to neuronal activity is an intensively studied subject, where optical techniques have been extraordinary successful. In this field, laser speckle imaging (LSI) has found widespread application, as it allows imaging of local changes in cerebral blood flow (CBF) with rather high spatial and temporal resolution [1–7].

Although the removal of the dura mater to access the brain cortex is still required in most cases, some groups perform imaging through the thinned skull of rats or through the intact

skull of mice. This has considerable advantages compared to the open skull experiments, as surgery is simplified and undesired side effects, such as cortical swelling, are avoided. However, the influence of the skull on the laser speckle signal has been quantitatively addressed only recently [8,9]. Here, we propose a refined processing scheme, which takes into account the effect of static contribution on the optical signal and thus allows for a correct computation of CBF. At the same time it does not require modifications of the typical laser speckle contrast analysis (LASCA) experimental settings and image acquisition procedure, which is a major advantage of our approach.

This paper is structured in two sections. The first part introduces the fundamentals of the optical signal and presents an advanced processing scheme for its appropriate evaluation. In the second part, data obtained from measurements of CBF in anesthetized rats are presented and the advantages of the refined processing scheme are demonstrated.

Materials and methods

Optical signal and processing

The method of LSI is a powerful - yet surprisingly simple - technique for the spatial two-dimensional mapping of localized dynamics. It is conceptually based on the dynamic light scattering methodology, were the fluctuations of the scattered light intensity are monitored with high temporal resolution and the dynamics of the medium is characterized through the temporal statistics of intensity fluctuations. In LSI temporal fluctuations are integrated during a relatively long camera exposure time leading to a partially blurred speckle image. Modern semiconductor detector arrays based on the CCD or CMOS technology are perfectly suited to analyze the resulting spatial intensity fluctuations: their temporal performance is rather limited, but the matrix size is sufficiently large. The physical picture is relatively straightforward: faster dynamics in some region leads to stronger blurring of the speckle pattern. When the "blurring" is quantified by an appropriate spatial statistical measure, such as contrast, it can be related to the time correlation properties of the intensity fluctuations. A map of the dynamics can be obtained by calculating the contrast locally, i.e. by dividing the camera matrix into rectangles of equal size and processing each rectangle independently. This is the basis of the widely recognized method termed laser speckle contrast analysis (LASCA).

The simplicity of the data interpretation and of the required instrumentation is among the major reasons for the high popularity of LSI in optical and biomedical communities. Numerous modifications, simplifications and optimizations appeared recently, some more focused on practical improvements of the image formation process [10–12] while others were addressing more fundamental questions related to the speckle statistical properties and the underlying temporal fluctuations [8,9,13–15] with the final goal to turn LSI into a "quantitative tool". One of the major pitfalls in LASCA is the fact that one needs to assume a particular shape of intensity correlation function in order to quantify the underlying dynamic processes. Moreover, the conversion of contrast can be made only for the simplest types of correlation function, while multi-parameter correlations cannot be analyzed. A particularly important example is the case in which detected light is composed of a fluctuating speckle field from moving scatterers and of static reflections from solid-like structures. The original LASCA is not able to account for the static component of the scattered field, which however often exists in in-vivo signals due to the structural complexity of tissue as a scattering system. Several recently published papers [8,13,16] explicitly stated that in order to improve quantitative reliability of LSI the model of the contrast signal formation could be refined. Parthasarathy et al. [8] and Smausz et al. [14] introduced the multi-exposure speckle imaging technique, where information obtained with different camera exposure times allows to characterize the underlying multi-parameter correlation function.

In our previous study [16], we have theoretically addressed the common case of multi-parameter correlation function, i.e. the presence of a static speckle pattern produced by the

rigid scattering structures in the detected image. We suggested that this effect could be accounted for with a relatively simple additional processing step: By cross-correlating sequentially acquired speckle images one can estimate the contribution of the non-fluctuating component to the total intensity. This quantity can then be used for the conversion of the speckle contrast to the correlation time.

Since this method constructs an image of the sample using the dynamic component of the speckle field only we refer to it as *dynamic laser speckle imaging (dLSI)* in contrast to general laser speckle imaging or LASCA. In this article we demonstrate the superior performance of dLSI for quantitative imaging the hemodynamic response in the rat brain cortex.

Theory

In LSI experiments the investigated medium is illuminated with coherent light (usually from a laser) and the obtained image is modulated by the random interference patterns called speckles produced by coherent addition of light diffusively scattered from the medium. Continuous displacement of scatterers in the medium leads to an alteration of the speckle pattern. An image is acquired with a camera during a certain time interval, called exposure time *T,* and the evolution of the speckle pattern during the camera exposure leads to the blurring of the speckle image or to a reduction of the local speckle contrast. The latter is defined as the standard deviation of the intensity divided by the mean:

$$K(T)=\frac{\sigma(T)}{\langle I\rangle}=\frac{\sqrt{\left\langle\left(I_T-\langle I_T\rangle\right)^2\right\rangle}}{\langle I_T\rangle} \qquad (1)$$

In the common LASCA approach [3,7,17] the image is divided into a set of rectangular areas and the contrast is calculated locally, thus providing a space-resolved map of the dynamics. One can quantitatively relate the contrast to the correlation properties of speckle fluctuations and to the characteristics of microscopic dynamics of moving scatterers. For the functional imaging of brain hemodynamics one can assume that the fluctuations of the speckle pattern originate from the microscopic movements of the red blood cells (RBC) in the microvascular system. Fluctuations of coherent light scattered by such a system can be described in the scope of the diffusing wave spectroscopy (DWS) model using the field correlation function $g_1(\tau)$ [18]:

$$g_1(\tau)=\exp\left(-\gamma\sqrt{6\tau/\tau_0}\right), \qquad (2)$$

which relates the temporal fluctuations of the scattered field amplitudes to the microscopic relaxation time τ_0 (for Brownian motion $\tau_0=1/Dk^2$ is given by the diffusion coefficient D and the wavenumber k), $\gamma\approx 1.5$ is a constant.

The DWS model can be applied to the case of blood flow in random directions and a broad velocity distribution of RBCs, which is representative for the motion in the brain microvascular structures (a more detailed discussion can be found *e.g.* in [13]).

The experimentally-accessible intensity correlation function $g_2(\tau)$ can be linked to the field correlation function $g_1(\tau)$ via Siegert relation [18,19]:

$$g_2(\tau)=1+\beta\left|g_1(\tau)\right|^2. \qquad (3)$$

Here β is the so-called coherence factor and $1/\beta$ is the effective number of speckle contributing to the intensity recorded by a given camera pixel.

At the same time, the contrast of the speckle image detected with exposure time T is related to the intensity and field correlation functions in the following manner:

$$K^2 = \frac{2}{T}\int_0^T \left[g_2(\tau)-1\right]\left(1-\frac{\tau}{T}\right)d\tau = \frac{2\beta}{T}\int_0^T \left|g_1(\tau)\right|^2\left(1-\frac{\tau}{T}\right)d\tau, \qquad (4)$$

Using Eq. (2) the correlation time τ_0 can be calculated from the measured contrast K via Eq. (4).

The reciprocal correlation time (RCT) of intensity fluctuations is often assumed to be proportional to the velocity of the scattering particles $1/\tau_0 \sim v$ [18,20]. This provides the quantitative basis for the interpretation of LASCA data. Equation (4) is often used to compute the velocity assuming that light scattering in the multiple scattering regime leads to the stretched-exponential form of the correlation function, as described by Eq. (2). In practice however, the scattering conditions might differ from the theoretical model of a pure homodyne detection and a mixing of the dynamic signal of interest with light scattered by static structures is possible. Indeed, it has been recently demonstrated that the use of traditional approaches to quantify $1/\tau_0$ can lead to a considerable error in the presence of a static contribution [9,19,21].

It is however possible to derive a rather simple formalism to deal with intensity fluctuations in the presence of a static component. We can define the static contribution as the light that has been scattered by rigid structures (such as bone or a skin layer which are not highly perfused with blood) only. The detected intensity in this case is composed of a non-fluctuating static part I_s and a dynamic part I_d with a relative static contribution to the total intensity: $\rho = \langle I_s \rangle / \left(\langle I_s \rangle + \langle I_d \rangle\right)$. In this case the correlation function of the mixed field can be written as a composition of the correlation function of the pure dynamic part $g_{1\mathrm{d}}(\tau)$ (Eq. (2)) and the time-independent baseline ρ from static light [9,22]:

$$g_1(\tau) = (1-\rho)\left|g_{1\mathrm{d}}(\tau)\right| + \rho. \qquad (5)$$

Using the Siegert relation we can find the intensity correlation function of the mixed signal:

$$g_2(\tau) - 1 = \beta\left[(1-\rho)\left|g_{1\mathrm{d}}(\tau)\right| + \rho\right]^2. \qquad (6)$$

Finally, the contrast of the superposition of static and dynamic speckles can be found by substituting Eq. (6) into Eq. (4):

$$\begin{aligned} K^2 &= \frac{2\beta}{T}\int_0^T \left[(1-\rho)\left|g_{1d}(\tau)\right| + \rho\right]^2 (1-\tau/T)\,d\tau \\ &= (1-\rho)^2 K_{2d}^2 + 2\rho(1-\rho)K_{1d}^2 + \beta\rho^2 \end{aligned} \qquad (7)$$

where the K_{2d} and K_{1d} represent the contrast of the dynamic intensity and the dynamic field respectively:

$$\begin{aligned} K_{2d}^2 &= \frac{2\beta}{T}\int_0^T \left|g_{1d}(\tau)\right|^2 (1-\tau/T)\,d\tau \\ K_{1d}^2 &= \frac{2\beta}{T}\int_0^T \left|g_{1d}(\tau)\right| (1-\tau/T)\,d\tau \end{aligned} \qquad (8)$$

Together K_{2d} and K_{1d} define the mixed dynamic part of the contrast:

$$K_{12d}^2 = \left(1-\rho^2\right) K_{2d}^2 + 2\rho\left(1-\rho\right) K_{1d}^2 \qquad (9)$$

If no static contribution is present ($\rho = 0$) the measured contrast reduces to: $K^2 \equiv K_{12d}^2 \equiv K_{2d}^2$. It the general case of $\rho > 0$ Eq. (7) represents the example of the multi-parameter correlation function, which cannot be quantitatively addressed with a general LASCA formalism. The ultimate solution for this problem might be the evaluation of the time-resolved intensity fluctuations for each pixel of the camera matrix with a microsecond resolution. Such an approach is computationally complex, requires both a high frame-rate camera and an excessively high incident laser power in order to cope with the corresponding short exposure times.

Alternatively, we have recently suggested a compromise solution [9,19,21], which preserves the simplicity by keeping the standard LASCA data acquisition scheme while accounting for the static or slow-drifting components in the signal. Here the static contribution ρ is calculated in an additional step of data processing, as discussed below.

In a LSI experiment the exposure time T (typically from 1 to 20 ms [23],) is chosen to be larger than the intensity correlation time τ_0 (in the range 0.001-0.1 ms for CBF). The time interval between successive frames Δt (in our case 20 ms) is larger than T and we find $\Delta t > T >> \tau_0$. This implies that essentially no correlations of the dynamic speckles are present on a time scale of Δt and thus $g_{1\,\mathrm{d}}\left(\Delta t\right) \approx 0$. Hence two speckle patterns detected in two sequential frames are correlated only due to the presence of static speckles. We can thus find the amount of static light in the detected signal by comparison of sequential frames and by making use of a multi-speckle averaging scheme [9,24,25].

With the dynamic correlation close to zero in Eq. (6) we can experimentally obtain the static contribution from the correlation of speckle patterns recorded in sequential camera frames:

$$\rho^2 = \left[g_2\left(\Delta t\right) - 1 \right] \Big/ \beta \qquad (10)$$

Since the contribution of the static light can be position dependent, ρ must be computed locally as well.

One can introduce the obtained ρ into Eq. (7) in order to relate the measured contrast K_m to the relaxation time τ_0 of the dynamic part of the correlation function defined in Eq. (2). This can be done numerically by calculating the function $K\left(\tau_0\right)$ using ρ . Instead of integrating the correlation function in Eq. (4), one can use the analytical expressions for the dependence of dynamic contrasts K_{1d} and K_{2d} on τ_0 , available for the most simple forms of field correlation function (such as single or stretched exponential) [25].

Thus, the procedure to calculate the correlation time including the correction for the static component can be divided into the following steps[1]:

1. Calculate the measured contrast: $K_m = \left[\dfrac{\left\langle I^2 \right\rangle}{\left\langle I \right\rangle} - 1 \right]^{1/2}$, where $\langle \cdots \rangle$ denotes the spatial averaging over a selected area containing N pixels: $\left\langle I \right\rangle = \dfrac{1}{N}\sum_{i=1}^{N} I\left(x_i\right)$ and $\left\langle I^2 \right\rangle = \dfrac{1}{N}\sum_{i=1}^{N} I^2\left(x_i\right)$. We have denoted this measured contrast with an index m ($K_m \equiv K$)

2. Estimate the static contribution from two sequential images $I_1(x_i)$ and $I_2(x_i)$ with $i = 1...N$ defining the same set of pixels as used in step 1: $\rho = \frac{1}{\beta^{1/2}}\left[\frac{\langle I_1 I_2\rangle}{\langle I_1\rangle\langle I_2\rangle} - 1\right]^{1/2}$,

where $\langle I_1 I_2\rangle = \frac{1}{N}\sum_{i=1}^{N} I_1(x_i)\cdot I_2(x_i)$. The β-factor used in this calculation has to be obtained separately. It can be calibrated using a solid white medium such as a block of Teflon or a sheet of paper with $\rho \equiv 1$.

3. With knowledge of ρ the mixed dynamic contrast $K_{12\,d}$ can be obtained with the following relation $K_{12\,\mathrm{d}}^2 = K_m^2 - \beta\rho^2$, which follows from Eq. (8). Using an appropriate model for the field correlation function $g_{1d}(\tau)$ (e.g. Eq. (3)) the characteristic relaxation time τ_0 can be extracted numerically from Eq. (10) as explained above.

Animal preparation

15 adult Sprague-Dawley rats (approx. 250 g) were used. Surgery was performed under isoflurane anesthesia, whereas during the actual experiment the rat was anesthetized with 44 mg / kg α-chloralose (s.c.). Catheters were placed in the right femoral artery and vein for the continuous monitoring of the arterial blood pressure (90 – 110 mm Hg) and for the administration of a lethal dose of pentobarbital at the end of the experiment. The animals were tracheotomized and mechanically ventilated to maintain physiological arterial levels of pH (7.35 – 7.45), pCO2 (34 – 38 mm Hg) and pO2 (>100 mm Hg). The body temperature was held constant at 37 degrees Celsius using a regulated heating pad. The animals were placed in a stereotactic frame (David Kopf Instruments, Tujunga, USA). For measurements through the intact skull, the skin was removed and the bone was carefully washed and bleedings from the bone were stopped using a mono-polar needle electrode driven by an electrosurgical instrument (Erbotom ICC 200, Erbe Elektromedizin GmbH, Tubingen, Germany). The skull was kept moist by covering it with agar (2% in saline). For the thinned bone preparation, the skull covering the left somatosensory cortex was carefully thinned to translucency using a surgical drill (Osseodoc, Bien Air, Biel, Switzerland). Finally, for imaging the exposed cortex, the bone and the dura mater were removed. The exposed cortex was then covered with agar.

A contralateral single vibrissa was deflected using a canula attached to a piezoelectric ceramic wafer (Piezo Systems Inc., Cambridge, MA, USA). A computer-triggered pulse (50 ms) sent to the wafer produced a 1 mm rostral to caudal deflection of the vibrissae. The stimulation lasted 4 s with a frequency of 4 Hz. Before stimulation, a baseline phase of 2 s was acquired. In each of the 15 animals, 10 trials were recorded and averaged with a 60 s inter-trial interval to allow the signals to return to baseline. The local veterinary authorities approved all experimental procedures.

Optical Imaging

Cortical images were acquired using a 12 bit CCD camera (Pixelfly VGA, PCO Imaging, Kelheim, Germany) attached to a motorized epifluorescence stereomicroscope (Leica MZ16 FA, Leica Microsystems, Heerbrugg, Switzerland) focused 0.5 mm below the cortical surface. Collimated 785 nm laser light was shown onto the cortex (TuiOptics, Munich, Germany). The images (640 x 480 pixels) were acquired with a frame rate of 50 Hz and an exposure time of 10 milliseconds. Circular regions of interest (ROIs) were drawn manually over the area of

maximal signal increase to extract the signal time courses. The 10 trials carried out in each animal were averaged. Values are converted to percent change from baseline before averaging across animals. All data represent the mean ± standard error of the mean of 5 animals used for each of the three experimental procedures.

Speckle images were processed first using the standard LASCA procedure and the measured contrast K_m and τ_0^{LASCA} were found using Eq. (4). The same data were evaluated with the dLSI algorithm: after calculation of the static component ρ with Eq. (10) the measured contrast K_m is inverted into the dynamical correlation time τ_0^{dLSI} using the obtained ρ according to the procedure described above.

Results

In order to evaluate the performance of the dLSI processing-scheme, we first analyze the speckle images of the exposed cortex. The procedure was similar to the one reported before [7].

Imaging of the exposed cortex

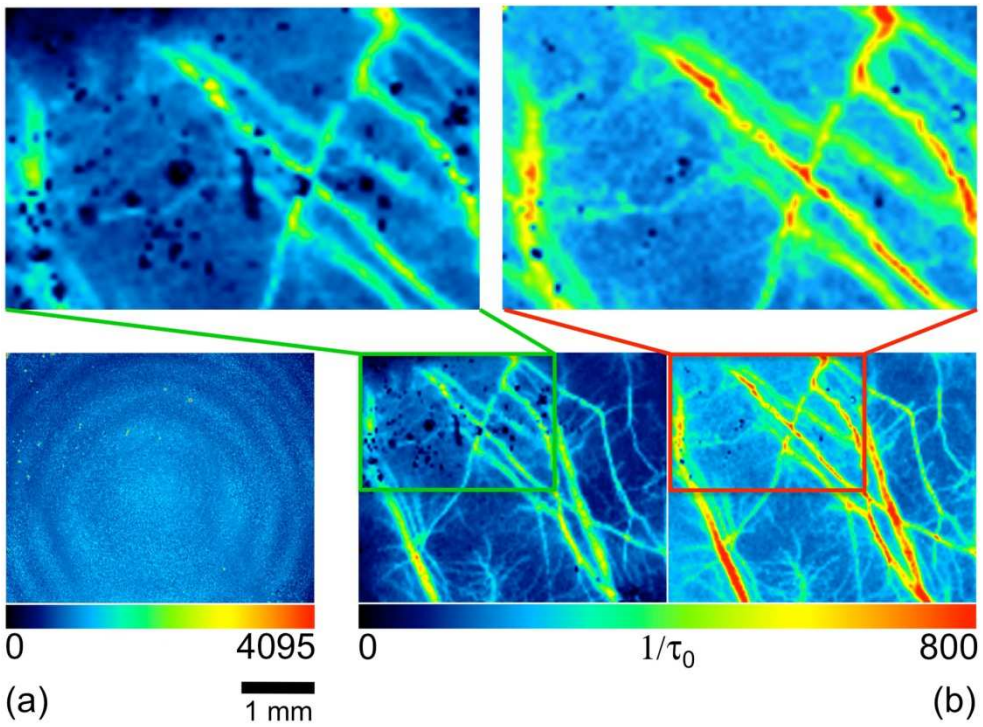

Fig. 1. (a): Raw speckle reflection recorded with 10 ms exposure time, measured through thinned skull. (b) left: Reciprocal correlation time (RCT) derived from classical LASCA. (b) right: RCT computed with dLSI. Note the substantial reduction of specular reflections in the right panel. RCT values represent averages over 32 consecutive images.

The comparison between the results obtained with standard LASCA (laser speckle contrast analysis) and the novel method is presented in Fig. 1. One can observe the typical glare from specular reflections of the cortical surface in the intensity images. The surface can be considered as static on the time scale of the measurement (10 milliseconds exposure time). LASCA processing results in extremely high contrast values in the areas of the specular reflection not because of the slower dynamics of RBCs but due to non-negligible static contribution to the contrast. However, with the help of dLSI processing, the surface

reflections are almost completely suppressed and the estimated sample dynamics in the area does not differ from the regions without glare (Fig. 1). Another feature of the images obtained with dLSI processing is the more pronounced differentiation of the regions with spatially non-uniform dynamics. For example the blood vessels are better distinguished from the cortex tissue using dLSI. This is a consequence of the removal of the static baseline from the dLSI images, which increases the dynamic range of the RCT compared to LASCA.

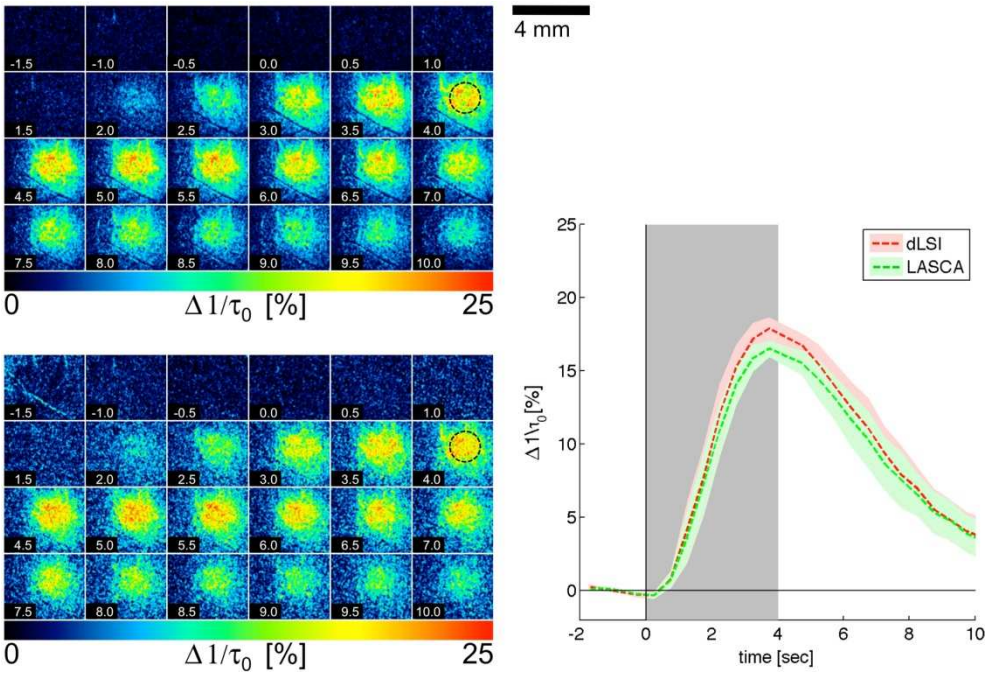

Fig. 2. Left: Example of activation maps obtained from an exposed cortex measurement. Maps represent relative changes of the reciprocal correlation time obtained from LASCA (top) and dLSI (bottom) signal upon single whisker stimulation (time step 0.5 s). The black dashed circle at second 4 shows the region-of-interest used for averaging the time activity curve. Right: Time activity curves averaged over 5 animals (10 trials each) from activated area (dashed lines show average, shaded area represents ± standard error of the mean). Gray area represents the duration of the whisker stimulation.

Figure 2 shows an activity map of the exposed cortex obtained from the total measured contrast with LASCA processing and from the dynamic contrast with dLSI processing. The region of increased blood flow can clearly be localized with both methods. Besides the somewhat higher amplitude of activation changes obtained with dLSI one can observe no major differences in the results. This is also supported by the time traces of relative changes shown in Fig. 2. The activation response of the dynamic signal is only slightly higher and reaches 17.90 ± 0.77% (right panel on Fig. 2) while the correlation time estimated with the LASCA method peaks around 16.53 ± 0.54%.

Table 1. Static contribution ρ, measured contrast K_m, baseline and change of reciprocal correlation time, obtained with LASCA and dLSI for three types of experiment (for details please see text).

		Exposed cortex	Thinned skull	Intact skull
ρ		0.060 ± 0.002	0.065 ± 0.002	0.171 ± 0.019
K_m	LASCA	0.110 ± 0.012	0.130 ± 0.007	0.230 ± 0.019
	dLSI	0.112 ± 0.013	0.124 ± 0.007	0.163 ± 0.012
$1/\tau_0$ [s^{-1}]	LASCA	226 ± 44	138 ± 13	36 ± 6
	dLSI	307 ± 60	213 ± 22	151 ± 27
$\Delta 1/\tau_0$ [%]	LASCA	16.53 ± 0.54	17.5 ± 3.0	4.2 ± 1.2
	dLSI	17.90 ± 0.77	20.4 ± 3.2	7.3 ± 1.6

Table 1 summarizes the parameters extracted from speckle imaging data for all experimental conditions. The baseline of the reciprocal correlation time (RCT) obtained with LASCA and with dLSI are 226 ± 44 s^{-1} and 307 ± 60 s^{-1}, respectively. The amount of static contribution (0.060 ± 0.002) is small and the LASCA and dynamic contrast are relatively close (0.110 ± 0.012 versus 0.112 ± 0.013).

Functional imaging through the thinned skull

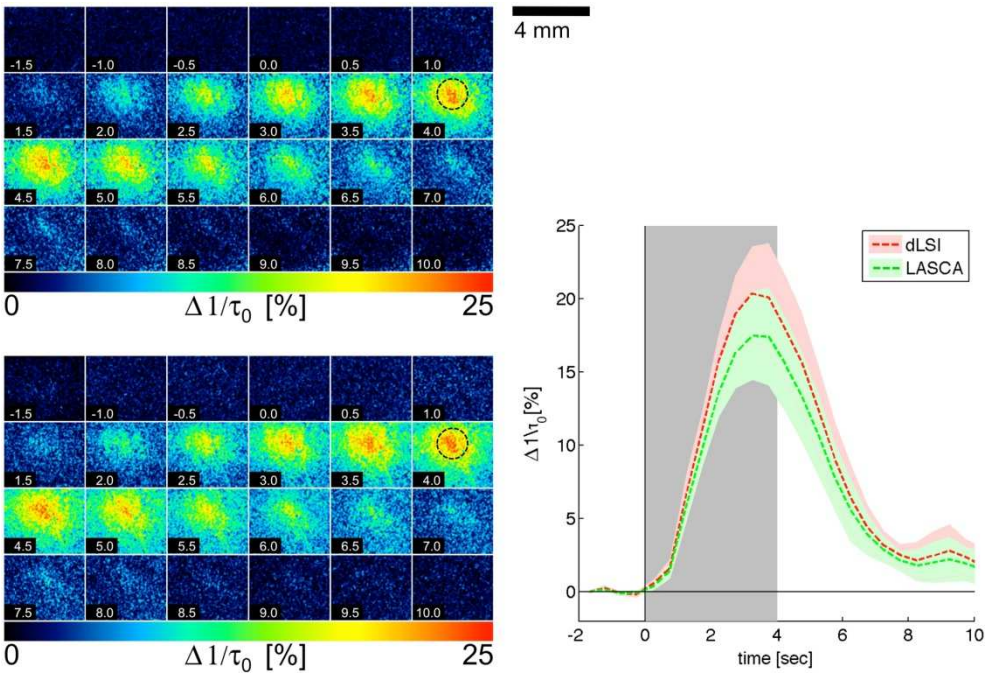

Fig. 3. Same as Fig. 2 but for thinned skull experiments.

Figure 3 shows the activation maps and the time curves for the imaging through the thinned skull. The static contribution is slightly higher (0.065 ± 0.002) for this case compared to the exposed cortex experiments. This is also true for the LASCA and dynamic contrast (0.130 ± 0.007 versus 0.124 ± 0.007). The baseline of the correlation time, estimated with dLSI is 213 ± 22 s^{-1}, while the LASCA estimate is lower 138 ± 13 s^{-1}. The maximal relative change of the reciprocal dynamic correlation time reaches 20.4 ± 3.2%, while it amounts to 17.5 ± 3.0% for the LASCA method, as can be seen in Fig. 3.

Functional imaging through the intact skull

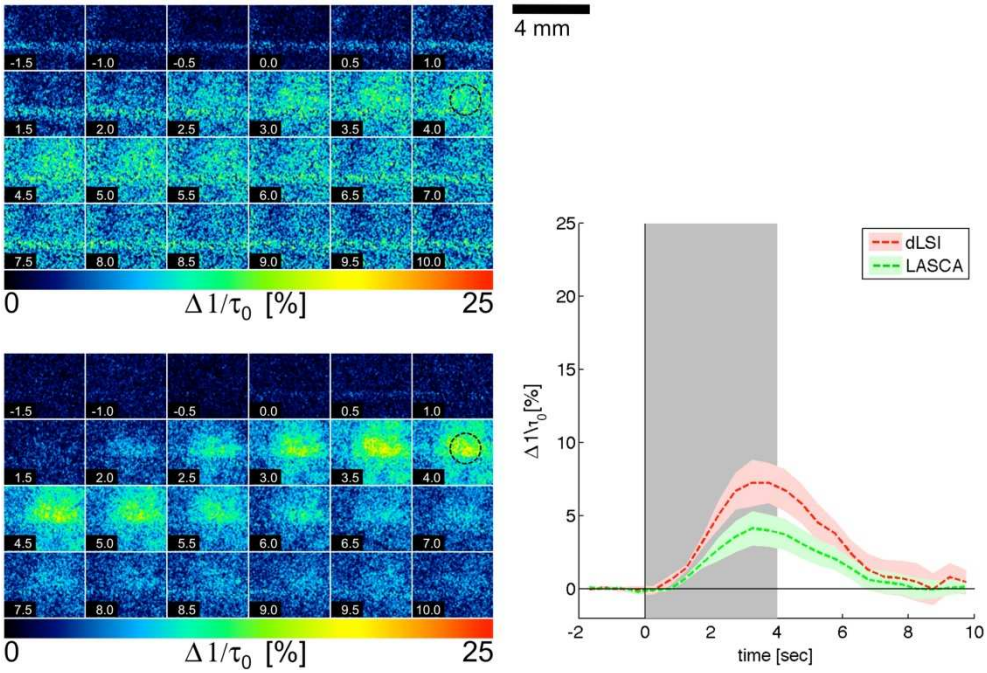

Fig. 4. Same as Fig. 2 and 3 but for experiments through the intact skull.

The activity map is shown in Fig. 4 together with the time curve. In this case an activation region can still be detected on the basis of the classic LASCA, but the location and shape is difficult to determine, since the activation response signal is distorted by noise. The dLSI map is however of considerably higher quality and one can easily recognize the shape of the response pattern. The signal change is also significantly larger for the dLSI map as shown in Fig. 4. The maximum relative change of RCT obtained with LASCA and dLSI differ by almost a factor of two (4.2 ± 1.2% and 7.3 ± 1.6%, correspondingly, see Table 1). The change of the dynamic signal obtained through the skull is nevertheless smaller than the one for the exposed cortex (17.9 ± 0.8%). The static part ρ reaches a value of 0.171 ± 0.019 for this case. The LASCA contrast and dynamic contrast deviates considerably (0.230 ± 0.019 and 0.163 ± 0.012, respectively), as well as the baseline of RCT, where the LASCA-based estimate is 36 ± 6 s^{-1}, while the dLSI RCT is much higher at 151 ± 27 s^{-1} and closer to the case of the exposed cortex (see Table 1).

Discussion

We have previously demonstrated in a model experiment that adequately taking into account the static contribution to the laser speckle image can help to reveal the true dynamical characteristics of the medium. This is true in particular when imaging needs to be performed through a highly scattering static medium such as the intact skull [9]. With the use of three different experimental preparations in the anesthetized rat, we demonstrate the superior performance of the newly proposed dLSI technique in practice.

Contribution of the static light

The contribution of the static component to the detected intensity as shown in Fig. 5 (a) grows with increased thickness of the bone layer with a minimum of ρ = 0.06 associated with the exposed cortex and reaching 0.17 for the intact skull, which is in agreement with the physical

picture of diffuse light reflection from a layered medium as well as with experimental results presented earlier [16]. With an increase of the bone thickness, the contribution of the light scattered from the skull to the detected intensity grows as can be observed in Fig. 5 (a). The smaller difference of the static contribution between the exposed case and the skull after thinning (around <0.1 mm thickness) as compared to the change for the intact skull case (around 0.35 mm) remains unclear. One of the possible reasons might be the low order scattering regime of the thinned skull, which by visual inspection appears almost transparent. The intact skull, in contrast, has a clear milky appearance, which indicates a multiple scattering regime. Due to preferential forward scattering within the bone [26] the amount of light scattered back by the thinned bone is relatively small, while for the intact skull the diffuse reflection starts to dominate. Thus, reduction of the skull thickness below the reduced scattering length leads to a considerable reduction the static contribution ρ, while further bone removal does not noticeably improve the dynamic signal.

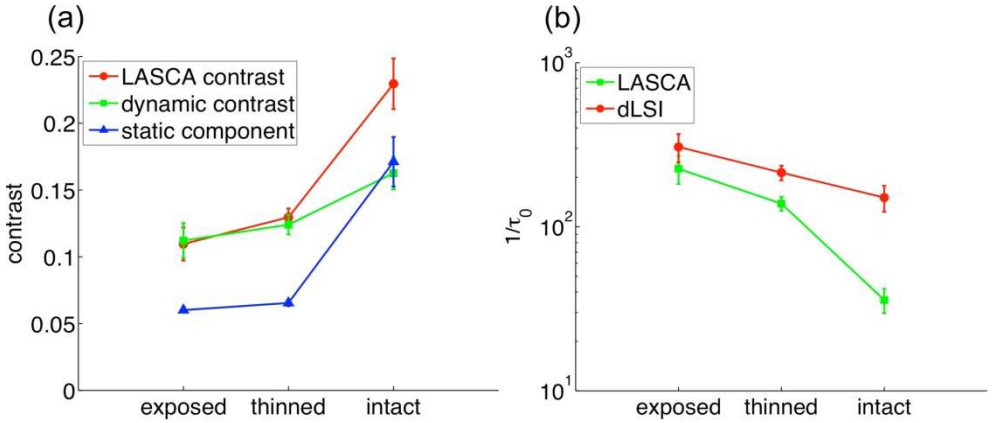

Fig. 5. (a): Static light contribution, LASCA contrast K_m and dynamic contrast K_{12d} for three different measurement methods during baseline (average ± standard error of the mean). (b): Reciprocal correlation time estimated with LASCA and dLSI for different measurement methods during baseline (average ± standard error of the mean).

Effect of the static light on the reciprocal correlation times obtained with LASCA

The larger the static intensity contribution the more the results from LASCA differ from dLSI as shown in Fig. 5 (b). For the intact skull measurements we find the LASCA-RCT almost 8 times smaller compared to dLSI. This striking result is in line with our previous modeling results, where an error up to 3 orders of magnitude has been demonstrated, if the contribution of static light is ignored in the processing [16]. Our results suggest that the dLSI substantially improves the accuracy of in-vivo laser speckle imaging.

It is worthwhile to note that even the dLSI can only partially overcome the inherent limitations of in-vivo measurements. This can be explained by the following arguments. In our model we separate the detected photons into two categories: dynamic and static. Our dLSI can thus distinguish between these two categories and provides a tool to analyze the local dynamics without being obscured by the presence of static light. However, the efficiency of the method is lower for in vivo conditions, since the skull cannot be regarded as static in the strict sense. Several factors, such as a low blood flow in the bone, movements of the animal due to breathing or temporal changes in the water content of the bone can produce relatively slow dynamics in the speckle pattern. As a result, the dLSI method underestimates the amount of static or pseudo-static contributions and the calculated correlation time must be considered an upper estimate for the actual value.

Functional response to the activation

We have demonstrated that dLSI provides a higher relative sensitivity to the functional activation than LASCA in all three experimental settings. As expected the improvement is most pronounced for the measurement through the intact skull (7.3% change against 4.2%, correspondingly). Only a marginal difference has been observed between the exposed cortex and the thinned skull measurements (17.9% against 16.5%).

However, even with our dLSI processing of the intact skull measurements we do not fully recover the response observed for the exposed cortex or thinned skull measurements. This might be due to the presence of slowly evolving speckles, as described above. Another influence should be related to a loss of intrinsic spatial resolution due to the photons that have traveled laterally through the cortex and the skull.

Some of the limitations discussed above might be partially addressed by analyzing additional lag times in dLSI, which would allow to better discriminate slow-evolving components from the intrinsic functional signal related to changes in cerebral blood flow. This can also be achieved by using a multi-exposure speckle imaging as proposed by Parthasarathy et al. [8]. Both approaches however require substantial modifications of the measurement setup and the data treatment. Further experiments are required to evaluate whether this increased complexity can be justified by quantitative improvements in the measured signal.

Finally we would like to comment on the following observation. The time course of the CBF change differs in the case of the exposed cortex as compared to the thinned and intact skull. Whereas in the latter cases the CBF returns to baseline within the 10 seconds, this is not the case for the exposed cortex. Further experiments are needed to investigate whether this is a robust effect and whether it might be caused by the perturbation of the cortex by the surgical intervention (e.g. release of pressure on cortex by removal of bone and dura mater).

Functional response to activation in the case of thinned skull

In the case of the thinned skull we have observed slightly higher response amplitudes than in the exposed cortex for both LASCA and dLSI. This result is somewhat surprising. However, it should be taken into account that after the skull thinning procedure the distance to the cortex is relatively small (around 0.20 mm), which apparently does not produce a sizeable static reflection as compared to the intact skull (see the discussion above). Nevertheless, it is associated with a higher contrast and slower hemodynamics (as shown in Figs. 2 and 5). We assume that the opening of the skull and dura performed for the imaging of the exposed cortex caused a slight increase of the baseline level of cerebral blood flow. Thus, the experimental stimulation could have provoked a smaller CBF increase and thus a lower signal change as compared to the results obtained through the thinned bone. For the thinned skull measurements a considerable part of the bone obstructing imaging has been removed, while the protective function of the skull and the dura is maintained and the cortex is minimally affected. Because of its less invasive character, many investigators have preferred the thinned skull preparation over the exposure of the cortex in optical imaging experiments [27–29].

In this case the dLSI processing can ensure a correct treatment of the contribution from static speckles produced by the remaining bone and dura. Taking this into account the thinned skull preparation shows an obvious advantage over procedures with complete removal of the skull or measurements through the intact skull, by providing the best compromise between invasiveness and quality of optical signal.

In summary, our results indicate that dLSI can indeed improve the quality of the activity maps obtained with laser speckles imaging through the intact and thinned rat skull. In accordance with the model experiments, we demonstrate that ignoring the static light contribution to the detected signal can lead to a large error in the estimated correlation times of the RBCs' movement. Decomposing the static and dynamic part with the proposed dLSI algorithm helps to improve the laser speckle signal sensitivity to the functional activation and

most importantly leads to a more accurate estimation of the hemodynamic response amplitude. Our results also suggest, that the thinned skull procedure, which reduces the obstructive effect of the bone on light propagation while preserving the brain cortex in a natural physiological state is the favorable surgical approach for laser speckle imaging of cerebral blood flow. In this case, the estimation of the static contribution with the use of the dLSI algorithm can be useful for the characterization of the impact of the residual bone and meninges on the LSI signal, and thus helps to obtain a more adequate quantification of the hemodynamic response.

Acknowledgements

We gratefully acknowledge the financial support by the Swiss National Science Foundation (Grants PP00B-110751/1, 200020-111824, 200020-117762 and 310000-11005) and by the OPO Stiftung. [1] The Matlab code for the above calculations can be obtained from the authors upon request.